Hybrid approach used for extended image-based wavefront sensor-less adaptive optics

Bing Dong (董 冰)* and Ji Yu (喻 际)

School of Optoelectronics, Beijing Institute of Technology, Beijing 100081, China
**Corresponding author: bdong@bit.edu.cn*

Received December 10, 2014; accepted January 16, 2015; posted online March 13, 2015

The stochastic parallel gradient descent (SPGD) algorithm is widely used in wavefront sensor-less adaptive optics (WSAO) systems. However, the convergence is relatively slow. Modal-based algorithms usually provide much faster convergence than SPGD; however, the limited actuator stroke of the deformable mirror (DM) often prohibits the sensing of higher-order modes or renders a closed-loop correction inapplicable. Based on a comparative analysis of SPGD and the DM-modal-based algorithm, a hybrid approach involving both algorithms is proposed for extended image-based WSAO, and is demonstrated in this experiment. The hybrid approach can achieve similar correction results to pure SPGD, but with a dramatically decreased iteration number.

OCIS codes: 110.1080, 110.3010.
doi: 10.3788/COL201513.041101.

In wavefront sensor-less adaptive optics (WSAO) systems, a distinct wavefront sensor is absent and a wavefront corrector is directly driven to optimize a metric function related to image quality. The control algorithms in WSAO can be divided into two categories: model-free algorithms and modal-based algorithms. Model-free algorithms like hill climbing[1], genetics[2], and stochastic parallel gradient descent (SPGD)[3] have been widely used in many scenarios. Their common disadvantages are that a large number of iterations are usually needed and a global convergence is not always guaranteed. In modal-based WSAO, the wavefront aberration is decomposed into specific modes like Zernike modes[4], Lukosz modes[5,6], or deformable mirror (DM) modes[7,8]. It has been demonstrated that DM modes are superior to analytical modes like the Lukosz modes, since the mode fitting error can be mostly avoided, especially for DMs with a low actuator number[7,8]. The modes' coefficients are calculated directly from the relationship between the mode coefficient and a proper metric function. Modal-based algorithms lead to a much faster convergence than model-free algorithms, and also avoid dropping into the local optimum.

Both model-free and modal-based algorithms can be adapted to a point-like source or an extended target. For high-resolution biological microscopy or earth observation purposes[9,10], wavefront aberration should be corrected from an extended image. In this Letter, the performances of the SPGD and the DM-modal-based algorithm used for extended image-based WSAO are evaluated and compared by simulation. From the simulation result, the advantages and drawbacks of the two algorithms are revealed. Then, a hybrid approach involving both of them is proposed to avoid drawbacks, and is further demonstrated by experiment.

SPGD is believed to be one of the fastest model-free algorithms. In a SPGD, small random perturbations are applied to all control parameters (voltages of actuators) simultaneously. Then, the gradient variation of a metric function is evaluated to update the search direction. The control signals are updated according to the following rule:

$$\mathbf{u}^k = \mathbf{u}^{k-1} + \gamma \delta \mathbf{u}^k \delta J^k, \tag{1}$$

where $\mathbf{u} = \{u_1, u_2, ..., u_N\}$ is the control signal vector, N is the number of actuators, and k is the iteration number. Here, γ is the gain factor, $\delta\mathbf{u}$ denotes small random perturbations that have identical amplitudes and Bernoulli probability distributions, and δJ is the variation of the metric function.

For extended image targets, several metric functions might be used in a SPGD[11]. Here, we use the normalized image sharpness function that is immune to intensity fluctuations in the light source and the sensitivity variation of the detector[12]

$$J = \frac{\sum I^2(x, y)}{\left(\sum I(x, y)\right)^2}, \tag{2}$$

where $I(x, y)$ is the intensity distribution at the image plane.

In modal-based WSAO, the low spatial frequency content of the extended-image spectral density $S_J(\mathbf{m})$ is used as the metric function[6,8]

$$g(M_1, M_2) = \int_0^{2\pi} \int_{M_1}^{M_2} S_J(\mathbf{m}) m \mathrm{d}m \mathrm{d}\xi, \tag{3}$$

where M_1 and M_2 are the normalized spatial frequencies, ξ is the angle of the spatial frequency, and $\mathbf{m} = (m \cos \xi, m \sin \xi)$. The relationship between the wavefront aberration $\mathbf{\Phi}$ and the metric function g is given by

$$g \approx q_0 - q_1 \frac{1}{\pi} \iint_p |\nabla \mathbf{\Phi}|^2 \mathrm{d}s, \tag{4}$$

where q_0 and q_1 are constants that depend on the object's structure. The wavefront aberration $\mathbf{\Phi}$ can be represented by a series of modes $\mathbf{Z}_i$, the derivatives of which are orthogonal with each other:

$$\mathbf{\Phi} = \sum_{i=4}^{N} a_i \mathbf{Z}_i, \tag{5}$$

$$\iint_p \nabla Z_i \cdot \nabla Z_j \mathrm{d}s = \begin{cases} 1 & i = j \\ 0 & i \neq j \end{cases}. \tag{6}$$

From the above, Eq. (4) can be rewritten in terms of the modes' coefficients as:

$$g = q_0 - q_1 \sum_{i=4}^{N} a_i^2. \tag{7}$$

The system's initial metric function is g_0. The metric function after introducing a positive modal bias $+b_i Z_i$ using a DM is g_+, and a negative modal bias $-b_i Z_i$ corresponds to g_-. The required correction amount of each mode is given by

$$a_{i,\mathrm{corr}} = -a_i = -\frac{b_i(g_+ - g_-)}{2g_+ - 4g_0 + 2g_-}. \tag{8}$$

To calculate certain mode coefficients, at least three measurements of the metric function are required, and $2N+1$ measurements should be taken for N modes correction.

The Lukosz modes satisfying Eq. (6) were initially used to describe the wavefront aberration[6]. However, the DM modes derived from the influence function matrix are more suitable in practice for wavefront correction, especially when the total actuator number is small[7,8]. The matrix consisting of the influence functions of all of the actuators is defined as $\boldsymbol{\omega}$. Its derivative matrix $\nabla\boldsymbol{\omega}$ can be converted into a multiplication of three matrices by singular value decomposition as

$$\nabla\boldsymbol{\omega} = (\nabla \mathbf{U})\mathbf{S}\mathbf{V}^{\mathbf{T}}. \tag{9}$$

The matrix $\mathbf{U}$ can be obtained from the integration of Eq. (9):

$$\mathbf{U} = \boldsymbol{\omega}(\mathbf{S}\mathbf{V}^{\mathbf{T}})^{-1}. \tag{10}$$

The columns of matrix $\mathbf{U}$ are derivative-orthogonal modes (i.e., DM modes) that also meet the requirements of Eq. (6). The DM modes are normalized by the root mean square (RMS) value. So a unit amplitude of the DM mode corresponds to a phase deformation with RMS = 1 rad, which is similar to the definition of standard Zernike polynomials.

In our simulation, a 37-channel DM model is built with a Gaussian-type influence function (coupling coefficient = 0.2). The dotted inner circle in Fig. 1 denotes the actual pupil size, which is reduced to about two-thirds of the DM aperture in order to obtain an optimized wavefront fitting result[13].

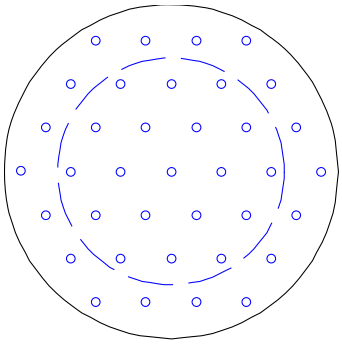

Fig. 1. The actuator arrangement of a 37-channel DM.

The extended imaging object is a typical remote sensing image, such as the one used in Ref. [8]. Input wavefront aberrations are generated by applying random driving signals to the DM actuators, which means that in theory, these aberrations can be fully corrected by the DM, so we can focus on the performance of the algorithms. The RMS values of these wavefront aberrations are then normalized to 1, 3, and 5 rad. For 100 wavefront error samples, the averaged residual wavefront RMS error after the correction of the SPGD and the DM-modal-based algorithm are shown in Figs. 2 and 3, respectively. From Figs. 2 and 3, we can see that, given sufficient iterations, the two algorithms both lead to satisfactory correction results. However, the required iteration number of the modal approach is much less than that of the SPGD.

Although it provides fast convergence, the modal approach has its drawbacks. First, the DM modes must be calibrated exactly by a wavefront sensor or an interferometer in advance, which is not a prerequisite for the SPGD. Second, the required mode bias amplitude

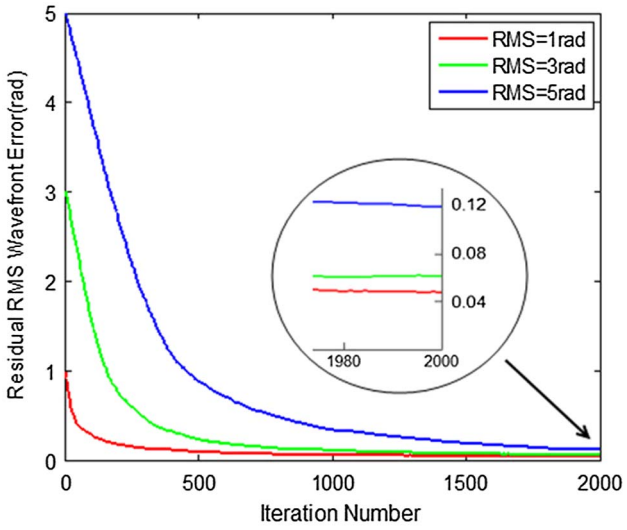

Fig. 2. The residual wavefront error varies with the iteration number in the SPGD correction.

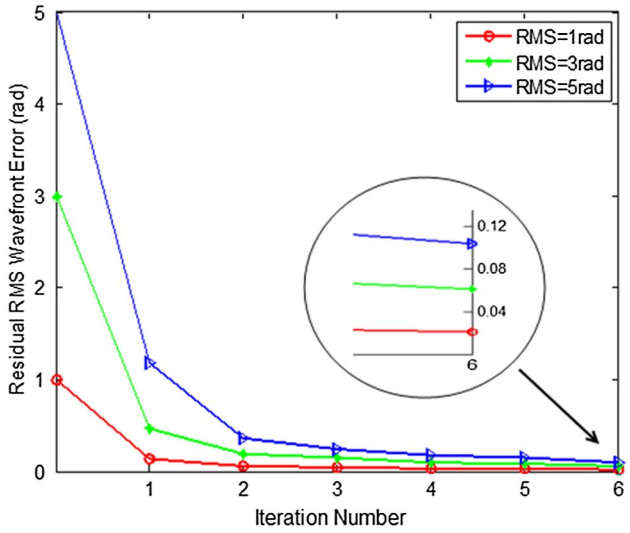

Fig. 3. The residual wavefront error varies with the iteration number in the DM-modal-based correction.

[b_i in Eq. (8)] is much larger than the random perturbation amplitude [amplitude of $\delta\mathbf{u}$ in Eq. (1)] in the SPGD. So in practice, the modal approach is more prone to a stroke saturation (or stroke insufficiency) problem, especially when producing some higher-order modes that require larger actuator signals[14,15]. The stroke saturation problem will prevent the sensing of some higher-order modes or render closed-loop correction inapplicable if the DM dynamic range is not large enough.

For a different mode bias amplitude, the residual wavefront error after a one-cycle correction is shown in Fig. 4. From Fig. 4, we can see that the optimized bias amplitude is around 1.5 rad. Here, the signal-to-noise ratio (SNR), which is defined as the ratio of the image variance to the noise variance, is set to 50. The bias amplitude can be even larger for a lower SNR. The peak-to-valley (PV) value of each DM mode with its unit amplitude ($b_i = 1$) is shown in Fig. 5. According to Fig. 5, to generate all 37 DM modes with amplitude of 1.5, the actuator

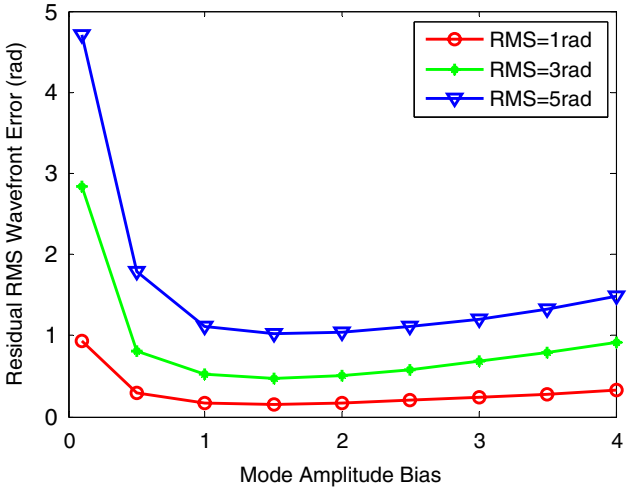

Fig. 4. The residual wavefront error varies with the mode bias amplitude. SNR = 50.

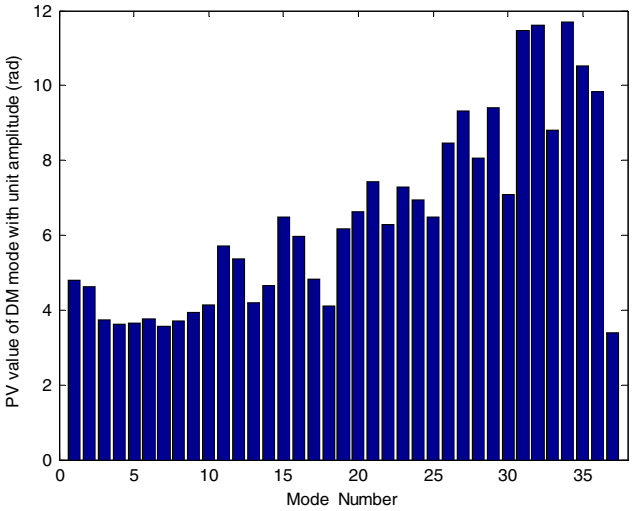

Fig. 5. The PV value of each DM mode with the unit amplitude.

stroke requirement is about 1.5λ. This requirement might be easily satisfied in first correction cycle. But the stroke will probably be insufficient for the next iteration when the input aberration is large. In the SPGD, the perturbation amplitude is 0.1 when SNR = 50 and the corresponding stroke requirement is about 0.03λ. So actuator stroke is generally not a limitation factor in SPGD. This issue is further illustrated later by experiment.

To avoid the stroke saturation problem in the modal-based algorithm, a hybrid approach involving both modal-based and modal-free algorithms is proposed. The hybrid approach is a two-step process. The wavefront aberration is first corrected by a modal-based algorithm and the residual error is further corrected by SPGD, which will take the phase estimation result of the modal-based algorithm as a good start point.

The hybrid approach has been demonstrated by experiment. The experimental system is depicted in Fig. 6. The insertable point light source is a 635 nm laser coupled with a single-mode fiber. The Shack–Hartmann wavefront

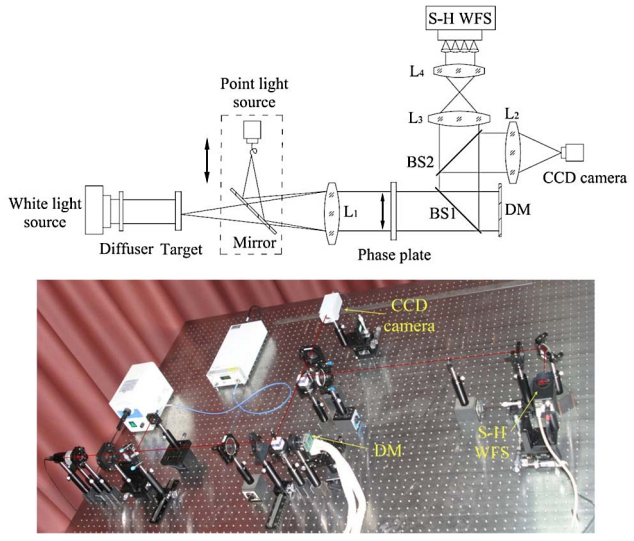

Fig. 6. The experimental system layout.

sensor (S–H WFS) from the Imagine Optics Corporation features 76×100 sub-apertures and $\lambda/100$ (RMS) measurement accuracy. Please note that here the S–H WFS is only used to measure the initial and residual wavefront errors and to calibrate the DM. It will not be used during the wavefront correction. The DM is a 37-channel membrane DM from the OKO International Company. The imaging target illuminated by the white light source is a 1951 USAF resolution test target. The insertable phase plate is a trial lens used to induce the wavefront aberration.

Before correction, the point light source branch is moved into the system and the influence functions of the DM are measured by the S–H WFS to deduce the DM modes according to Eq. (10). The DM modes were already illustrated in Ref. [8]. Then, the phase plate is inserted into the system. The initial wavefront error and corresponding distorted image are shown in Fig. 7.

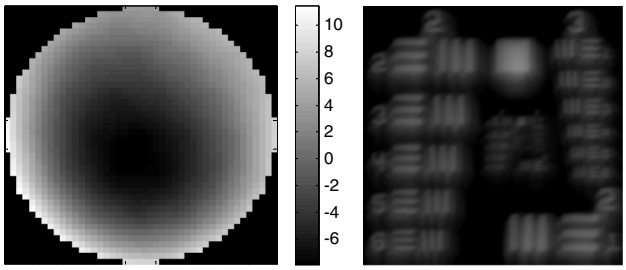

Fig. 7. The initial wavefront error (PV = 19.2 rad and RMS = 4.3 rad) and the corresponding image.

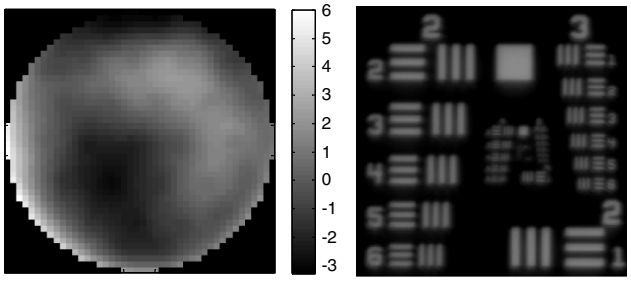

Fig. 8. The residual wavefront error after a one-cycle correction of the DM-modal-based algorithm, where PV = 9.12 rad, and RMS = 1.48 rad. Image after correction (right).

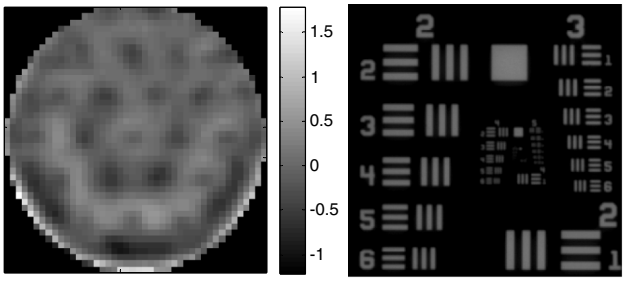

Fig. 9. The residual wavefront error after the SPGD correction, where PV = 2.87 rad and RMS = 0.26 rad. Image after correction (right).

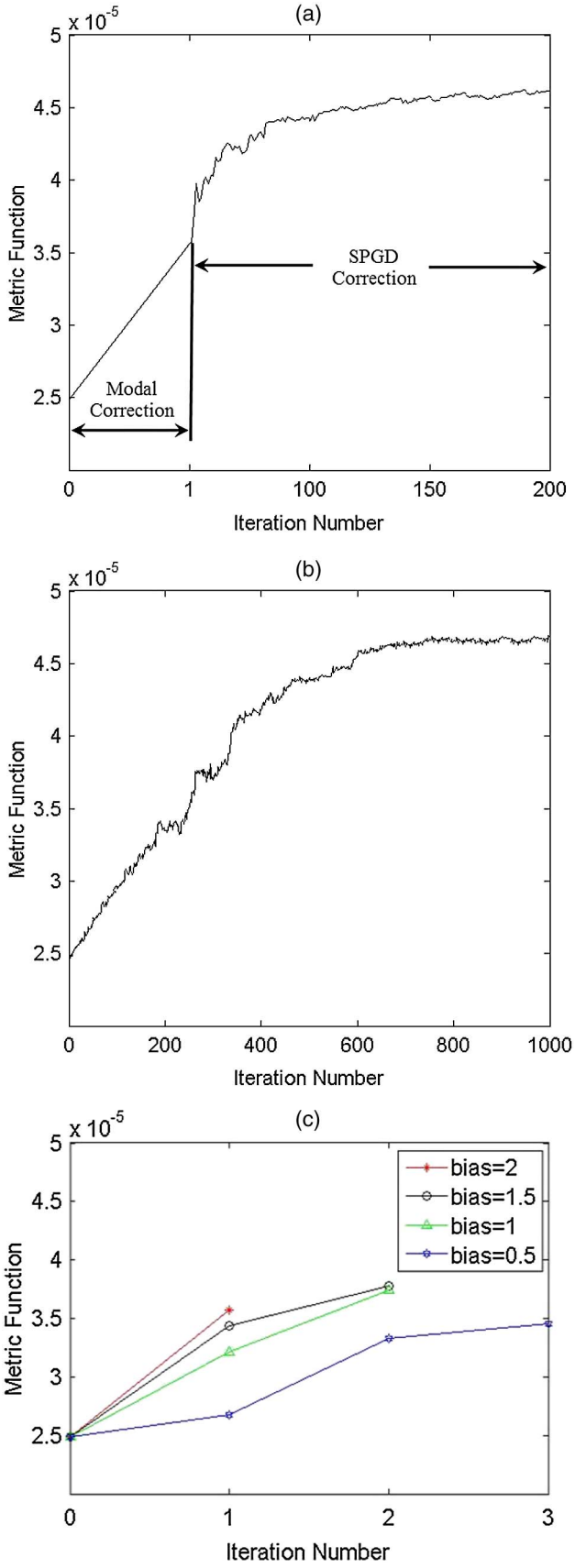

Fig. 10. The metric function-changing curve. (a) The hybrid correction. (b) The only SPGD correction. (c) The only modal correction with a different bias amplitude (unit: rad).

In hybrid correction, the wavefront error is first corrected by DM-modal-based algorithm. Then, the SPGD algorithm is applied to refine the correction results. The correction results and related images are shown in Figs. 8 and 9.

The changing curve of the metric function [Eq. (2)] during hybrid wavefront correction is shown in Fig. 10(a). The metric function-changing curves from using the SPGD and modal approach alone are plotted for comparison in Figs. 10(b) and 10(c), respectively. In Fig. 10(c), the modal correction process with different bias amplitudes are illustrated. Iterative correction is prohibited because of the stroke saturation problem, as discussed before. With a bias amplitude of 2 rad, iterative correction is stopped after one cycle. The convergence value of the hybrid correction and the SPGD is very close to 4.6×10^{-5}. However, the iteration number of the hybrid correction is dramatically decreased from 1000 to 200.

In conclusion, we experimentally demonstrate a hybrid approach involving both a DM-modal-based algorithm and the SPGD for extended image-based WSAO. The actuator-saturation problem in modal-based correction is solved by the SPGD correction. The convergence of the hybrid approach is much faster than SPGD alone because it uses a good starting point originating from the modal correction result.

This work was supported by the Specialized Research Fund for the Doctoral Program of Higher Education (Grant No. 20131101120023) and the Excellent Young Scholars Research Fund of the Beijing Institute of Technology (Grant No. 2012YG0203).

References

1. C. Chang, L. Cheng, H. Su, Y. Y. Hu, K. Cho, W. Yen, C. Xu, C. Y. Dong, and S. Chen, Biomed. Opt. Express **5**, 1768 (2014).
2. P. Yang, Y. Liu, W. Yang, M. Ao, S. Hu, B. Xu, and W. Jiang, Chin. Opt. Lett. **5**, 497 (2007).
3. X. Li, X. Dong, H. Xiao, X. Wang, and X. Xu, Chin. Opt. Lett. **9**, 101401 (2011).
4. M. J. Booth, Opt. Express **14**, 1339 (2006).
5. M. J. Booth, Opt. Lett. **32**, 5 (2007).
6. D. Debarre, M. J. Booth, and T. Wilson, Opt. Express **15**, 8176 (2007).
7. B. R. Wang and M. J. Booth, Opt. Commun. **282**, 4467 (2009).
8. J. Yu and B. Dong, **34**, 1228001 (2014).
9. Y. Yu and Y. Zhang, Chin. Opt. Lett. **12**, 121202 (2014).
10. X. Tao and F. Yan, Chin. Opt. Lett. **12**, 042802 (2014).
11. H. Yang, X. Li, C. Gong, and W. Jiang, Opt. Express **17**, 3052 (2009).
12. Y. N. Sulai and A. Dubra, Biomed. Opt. Express **5**, 3059 (2014).
13. G. Vdovin, O. Soloviev, A. Samokhin, and M. Loktev, Opt. Express **16**, 2859 (2008).
14. E. Dalimier and C. Dainty, Opt. Express **13**, 4275 (2005).
15. K. Morzinski, B. Macintosh, D. Gavel, and D. Dillon, Opt. Express **17**, 5829 (2009).